Chapter 4

Analysis of Competing Failure Mechanisms in Layer Transferred Thin Films

4.1 Introduction

In this chapter, we develop the criterion for successful layer transfer from a thin film mechanics standpoint. To insure proper thin film exfoliation, samples of lithium niobate were implanted with hydrogen and helium based on the criterion developed in Chapter 3. The analysis of transverse cracks, often observed in thin films obtained by the layer transfer technique, is done for films in a state of tensile and compressive stress. The level of stress imposed on the film during heating due to the mismatch in thermal expansion coefficients between the substrate and thin film is shown to be the dominent factor in determining the quality of the transferred layer. In particular, it is shown that if the film is submitted to a tensile stress, the microcracks produced by ion implantation are not stable and deviate from the plane of implantation, causing the layer transfer process to fail. Conversely, if the transfered layer is in compressive stress exceeding a threshold value, then the film can buckle and delaminate, leading to transverse cracks induced by bending. As a result, we show that the imposed stress σ_m - which is determined by the temperature to which the samples are heated - must be within the range $-\sigma_c < \sigma_m < 0$ to produce an intact thin film where σ_c depends on the interfacial fracture energy and the size of defects at the interface between film and substrate. [1]

[1] This chapter is based on work done with Dr. Laurent Ponson who was the lead author on this paper. The theory portion of this chapter was derived by Dr. Ponson after joint discussions and the experimental verification of this theory was done by myself [94].

4.2 Layer Transfer and Lithium Niobate

Various applications in electronics and optics require the synthesis of high quality, defect-free single crystals on a substrate of a different material. Diverse heteroepitaxial growth processes have been proposed e.g., Reference [16], but these methods impose severe restrictions on the film/substrate combinations. Recently, the layer transfer process has been proposed and shows promise as an alternative when the film/substrate pair is very different [22, 87]. However, for some systems and heating conditions, undesirable transverse cracks are also produced in the thin film during the process. This phenomenon renders the transferred thin film useless for applications in microelectronics and others fields. Therefore, understanding the origin of such cracks is crucial to avoid their formation. Identifying quantitatively the conditions and the systems that are advantageous to nucleate undesirable cracks will help to define the limitations of the layer transfer process and to design possible solutions to overcome these limitations. This motivates the present analysis and the mechanism of formation of these undesirable cracks is the central point of this study.

In Section 4.3, the geometry used during the layer transfer process as well as the state of stress in the film are described. Then, a first possible origin of thin film failure is investigated in Section 4.4: the stability of cracks nucleating from defects introduced by ion implantation is analyzed, and we show that these cracks only propagate parallel to the film/substrate interface when the transfered film is in a state of compressive stress. In Section 4.5, we show that excessive compressive stress in film can lead to cracking by buckling, delamination, and then failure of the film. For a given system with fixed film thickness, this analysis provides an acceptable range for the compressive stress and as a result, limitations on the heating temperatures used during layer transfer. In Section 4.6, these theoretical predictions are combined with experimental observations made on a lithium niobate film bonded to a silicon substrate. The two failure mechanisms previously proposed are clearly identified in an analysis of the specimen after layer transfer. The theoretical criterion for good layer transfer ($-\sigma_c < \sigma_m < 0$) is found to agree with experimental observations.

4.3 Geometry of the System and Stress State of the Film

To perform layer transfer, the material to be cut is bonded on a substrate as shown in Figure 4.1. A bonding layer, observed to improve adhesion and avoid undesirable cracking for some systems, is also shown. Its influence on the whole system is limited to the interface properties between film and substrate (fracture energy and defect size) so that this interlayer can be neglected

in the following analysis without loss of generality. Such a layered system is then submitted to an elevated temperature ΔT and microcracks can nucleate in the plane of hydrogen and helium ion implantation within the film. This is represented as a dashed plane in Figure 4.1. When these microcracks coalesce, the bulk single crystal is separated from the transferred thin film with thickness h.

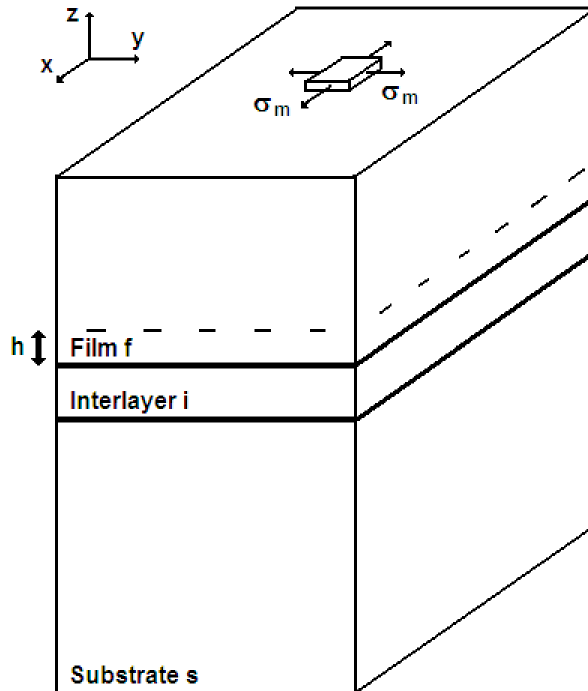

Figure 4.1. Geometry and stress field of the layered system. The dashed plane coincides with the plane of ion implantation and the thickness of the transfered layer, h, corresponds to the depth of ion implantation.

During the heating phase of the process, the film is submitted to a homogeneous biaxial stress σ_m caused by the mismatch in thermal expansion between the film and the substrate. Noting $\Delta\alpha = \alpha_s - \alpha_f$, the difference between the linear thermal expansion coefficients of the substrate and the film, one can show that irrespective of the thickness and thermal properties of the bonding layer, that the stress in the film is given by [44]:

$$\sigma_m = \frac{E}{1-\nu}\Delta T \Delta\alpha \tag{4.1}$$

where E and ν are the Young's modulus and the Poisson's ratio of the film, respectively. We will

see that to ensure transfer of a thin film without undesirable transverse cracks, the stress imposed on the film must be within a certain range of values to be determined in Sections 4.4 - 4.7.

4.4 Stability of Microcracks in the Film

We first focus on the trajectory of microcracks that initiate from the defects induced by the presence of hydrogen and/or helium in the specimen. To result in layer transfer, these microcracks are expected to propagate in a relatively straight manner, i.e., parallel to the interface between the film and the substrate. The stability analysis of a one-dimensional (1D) crack propagating in a two-dimensional (2D) elastic medium submitted to an internal stress was performed by Cotterell and Rice [27]. To apply this result to the layer transfer process, we should make the hypothesis that the behavior of the three-dimensional (3D) system as represented in Figure 4.1 is analogous to that of a cut of the full system along a plane perpendicular to the film/substrate interface, e.g., the plane (OYZ). In other words, we should suppose that the 2D penny-shaped microcracks propagating in the plane of ion implantation of the film can be approximated by 1D crack lines. This simplification is *a priori* not obvious, and in the following, we will study the propagation of a 2D crack in a 3D elastic medium. Figure 4.2 represents a part of the crack front of a 2D penny-shaped microcrack when observed at a sufficiently small scale so that the crack front appears roughly straight. The average front is taken parallel to the z axis of the local coordinates (O_{xyz}) and propagates along the x axis. As a result, the crack propagates in a plane parallel to (x, z), i.e., parallel to the interface between the film and the substrate. The question we address here is whether the crack will go on propagating within a plane parallel to (x, z) or will deviate from the straight trajectory because of the deflections generated by local heterogeneities in the film such as those induced by ion implantation. To proceed to such a stability analysis, we slightly perturb the crack front with respect to the straight geometry and study if those perturbations will tend to zero or will diverge while the crack is propagating. We define both out-of-plane perturbations $f(x, z)$ (along the y axis) and in-plane perturbations $g(z, t)$ (along the x axis) that are represented in Figure 4.2.

One can show that for small deflections, only the out-of-plane perturbations $f(x, z)$ are relevant to determine the local shearing $K_{II}(x, z)$ at the crack tip and, hence, the trajectory of the crack [62]. Let us note that the following analysis is independent of the shape of the small crack perturbations and remains valid whatever the choice of g and f are. To predict the crack trajectory, we apply the principle of local symmetry [27, 45, 49]: locally, at every point of the front $M(x, f(x, z), z)$, the

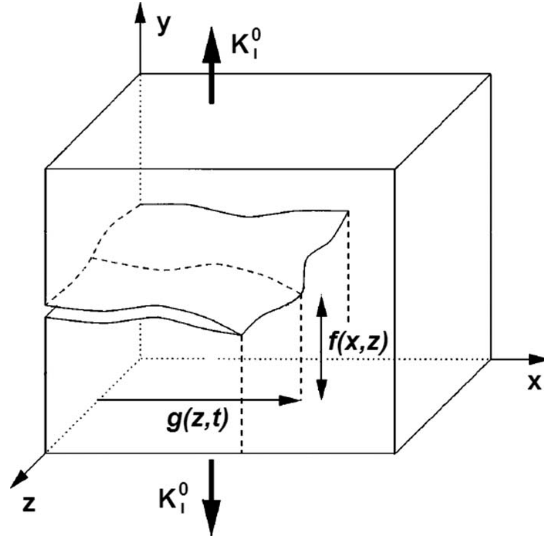

Figure 4.2. Geometry of a slightly perturbed crack propagating in the film.

crack propagates in a pure mode I opening state of stress. This condition is written as:

$$K_{II}[M(x, f, z)] = 0 \tag{4.2}$$

Movchan *et al.* [75] calculated the mode II stress intensity factor of a slightly perturbed crack propagating in an infinite 3D elastic medium for any perturbation $f(x)$.[2] Using their result, the local mode II stress intensity factor of cracks propagating in the ion implanted plane of the specimen can be expressed as:

$$K_{II} = \frac{K_I^0}{2} \frac{\partial f}{\partial x}\bigg|_{(x,z)} - \frac{K_I^0}{2\pi} \frac{2-3\nu}{2-\nu} \int_{-\infty}^{+\infty} \frac{f(x,z') - f(x,z)}{(z'-z)^2} dz' + \Delta K_{II}^{memory} \tag{4.3}$$

where the *memory* term K_{II}^{memory} is given by:

$$\begin{aligned} \Delta K_{II}^{memory}(x,z) &= -\int_{-\infty}^{x}\int_{-\infty}^{+\infty} \Big\{ w_x^{II}(x-x', z-z') \left(\tfrac{\partial (fT_{xx})}{\partial x}|_{(x',z')} + \tfrac{\partial (fT_{xz})}{\partial z}|_{(x',z')} \right) \\ &+ \ w_z^{II}(x-x', z-z') \left(\tfrac{\partial (fT_{xz})}{\partial x}|_{(x',z')} + \tfrac{\partial (fT_{zz})}{\partial z}|_{(x',z')} \right) \Big\} dx'dz' \end{aligned} \tag{4.4}$$

[2]Here, mode I stress is defined as tensile stress normal to the plane of the crack and mode II stress is defined as shear stress parallel to the crack plane and perpendicular to the crack front.

with

$$\begin{aligned} w_x^{II}(x,z) &= \tfrac{\sqrt{-2x}H(x)}{\pi^{3/2}*(x^2+z^2)}\left(1+\tfrac{2\nu}{2-\nu}\tfrac{1-(z/x)^2}{1+(z/x)^2}\right) \\ w_z^{II}(x,z) &= \tfrac{\sqrt{-2x}H(x)}{\pi^{3/2}*(x^2+z^2)}\tfrac{2\nu}{2-\nu}\tfrac{2z/x}{1+(z/x)^2} \end{aligned} \tag{4.5}$$

where $H(x)$ is the Heaviside function. In the preceding expressions, K_I^0 represents the average mode I stress intensity factor applied to the crack by the heated gas in the microcavities, while T_{xx}, T_{zz}, and T_{xz} are the T-stress terms or constant stresses imposed on the film in the absence of cracks. This implies that $T_{xx} = \sigma_m$, $T_{zz} = \sigma_m$, and $T_{xz} = 0$. Equation 4.3 provides the different contributions to the mode II shearing at a point M of the crack front induced by the perturbations of the fracture surface. The first term in Equation 4.3 corresponds to the contribution of the local slope along the propagation direction, while the second term provides the shearing induced by perturbations of the crack front. The third term, also referred to as the memory term, gives, as indicated by its name, the mode II contribution induced by the out-of-plane deviations of the crack line between its point of initiation and current position. This term is expressed as a function of the internal stress σ_m in the film, using the full expression of Equation 4.4 and changing T_{xx}, T_{zz}, and T_{xz} by their relevant expressions. Isolating the first term proportional to the local slope of the crack surface, the expression of the crack path, as given by the principle of local symmetry of Equation 4.2, can be rewritten as:

$$\begin{aligned} \tfrac{\partial f}{\partial x}\Big|_{(x,z)} &= \tfrac{1}{\pi}\tfrac{2-3\nu}{2-\nu}\int_{-\infty}^{+\infty}\tfrac{f(x,z')-f(x,z)}{(z'-z)^2}dz' \\ &+ \sigma_m\tfrac{2}{K_I^0}\int_{-\infty}^{x}\int_{-\infty}^{+\infty}\left(w_x^{II}(x-x',z-z')\,\tfrac{\partial f}{\partial x}\Big|_{(x',z')} + w_z^{II}(x-x',z-z')\,\tfrac{\partial f}{\partial z}\Big|_{(x',z')}\right)dx'dz' \end{aligned} \tag{4.6}$$

This equation predicts the crack path and so the stability of the failure process: let us take a perturbation of the crack oriented along the positive y axis so that $f > 0$. If $\frac{\partial f}{\partial x} < 0$, the local perturbation $f(x,z)$, is rapidly suppressed during crack propagation, and the crack surface is on average flat. On the other hand, if $\frac{\partial f}{\partial x} > 0$, even a small perturbation will grow and will lead to a macroscopic deviation of the crack from the (x,z) plane parallel to the interface. In the latter case, crack propagation becomes unstable. This situation will clearly lead to catastrophic transverse cracks in the thin film during the layer transfer process.

Next, we assess the relevance of each term of the righthand side of Equation 4.6 that determines the stability of microcracks in the film during heating. The first term acts as a nonlocal restoring force along the crack front that tries to maintain a straight trajectory. However, this term does

not prevent the crack from deviating from the mean crack plane[3] and therefore does not contribute directly to the stability of the crack. The second term is composed of a part proportional to $\frac{df}{dx}$ and another part proportional to $\frac{df}{dz}$. To assess the relative importance of each term, one can compare their two prefactors, w_x^{II} and w_z^{II}, respectively. According to Equation 4.5, w_z^{II} is smaller than w_x^{II}[4], and for most values of (z, x), one gets $\frac{w_x^{II}}{w_z^{II}} \ll 1$. In other words, the stability of the crack is mainly dictated by the term proportional to $\frac{df}{dx}$, leading to the approximation:

$$\left.\frac{\partial f}{\partial x}\right|_{(x,z)} \simeq \sigma_m \frac{2}{K_I^0} \int_{-\infty}^{x} \int_{-\infty}^{+\infty} w_x^{II}(x - x', z - z') \left|\frac{\partial f}{\partial x}\right|_{(x',z')} dx' dz' \quad (4.7)$$

From this equation, one can assess the evolution of the local slope of the crack surface. From Equation 4.5, one notes that $w_x^{II} > 0$. Therefore, the sign of σ_m will determine the evolution of the solution of Equation 4.7. If $\sigma_m > 0$, then $\left|\frac{\partial f}{\partial x}\right|$ is expected to increase when the crack propagates, while with $\sigma_m < 0$, $\frac{\partial f}{\partial x}$ will tend to zero after a finite distance.[5]

From analysis of the stability of a crack propagating during heating, one obtains:

(i) If the thin film is in a state of tensile stress ($\sigma_m > 0$), then the microcracks nucleated from the damage induced by ion implantation during the heating phase will deviate from the plane of implantation. One can therefore expect transverse cracks within the transferred thin film from systematic deviations of these microcracks.

(ii) If the film is in a state of compressive stress ($\sigma_m < 0$), then the microcracks are expected to propagate along a straight trajectory within the plane of ion implantation and will result in the transfer of a crack-free single crystal thin film. This compressive stress state is obtained if the thermal expansion coefficient of the film is larger than that of the substrate [see Equation 4.1].

As a result, the condition $\sigma_m < 0$ is necessary to obtain straight crack propagation and therefore an intact thin film. Let us note that this result is not limited to multilayer systems and can be extended to other systems where the crack trajectory needs to be analyzed: a 2D crack will remain

[3] For example, one can consider a crack with a perfectly straight front $f(x, z) = f(x)$. In that case, this term equals zero but f can be arbitrarily large, leading to unstable crack propagation.

[4] One can show that $\frac{w_z^{II}(x,z)}{w_x^{II}(x,z)} \leq \frac{2\nu}{2-\nu}$.

[5] For example, one can derive Equation 4.7 with respect to the variable x. Considering an initial perturbation $\frac{\partial f}{\partial x} > 0$, the sign of $\frac{\partial (\frac{\partial f}{\partial x})}{\partial x}$, and therefore the stability of the crack - positive (respectively, negative) for an unstable (respectively, stable) crack - is then provided by the sign of σ_m.

confined to a plane perpendicular to the external tensile loading if the stress is in compression along all the directions of this plane, while it will deviate from the straight trajectory if the stress is tensile along the mean plane of the crack. This analysis shows that the stability criterion shown for 2D elastic solids under mode I loading [27] remains valid for 3D systems. In Section 4.5, we will investigate another possible origin of film cracking and show that there is a limit to the amount of compressive stress the film can support, and an excessively high compressive stress in the film can also lead to poor quality transferred thin films.

4.5 Buckling, Delamination, and Failure of the Film

Here, another possible mechanism for film cracking during layer transfer process is investigated. Previously, we have shown that a state of tensile stress in the crystal containing the implanted plane must be avoided to ensure proper layer transfer. Therefore, systems with negative mismatch $\Delta\alpha = \alpha_s - \alpha_f$ between thermal expansion coefficients of the substrate and the film will be advantageously chosen. As an indirect consequence, the thin film freshly obtained may undergo a high compressive stress $\sigma_m < 0$, as given by Equation 4.1.

It is well known that thin films under compression can buckle and delaminate [44, 52]. We will see that these processes can have catastrophic consequences because it can lead to film failure by bending. The conditions leading to buckling, delamination, and failure of the film produced by layer transfer and subjected to a compressive stress σ_m are investigated in detail in Sections 4.5.2, 4.5.3, and 4.5.4, respectively. The film is supposed to be perfectly brittle so that the equations of elasticity for thin plates can be used. In addition, in first approximation, the fracture energy G_c of the film/substrate interface is assumed to be constant and independent of the phase angle $\phi = \arctan\left(\frac{K_{II}}{K_I}\right)$ of the stress acting on the interface [44].

4.5.1 Delamination of a Film with a Semi-Infinite Defect

Under compressive stress, a film bonded to a substrate can delaminate in order to release its internal stress. For an infinite film bonded to an infinite rigid substrate with a straight delamination front separating the film into two semi-infinite bonded and debonded parts, the elastic energy released during the propagation over a unit area is given by [44]:

$$G_{del} = \sigma_m^2 \frac{h}{2} \frac{1-\nu^2}{E} \tag{4.8}$$

where h, E, and ν are the thickness, the Youngs modulus, and the Poissons ratio of the film, respectively. Let us note that we do not consider cases where the substrate modulus is appreciably smaller than that of the film. This situation has been considered elsewhere [126]. Noting G_c the interfacial fracture energy between the film and the substrate [or the bonding layer if it has been added to the system (Figure 4.1)], one can use the Griffith criteria $G_{del} = G_c$ providing the onset of crack propagation to get an expression of the critical stress del for delamination,

$$\sigma_{del} = \sqrt{\frac{2EG_c}{h(1-\nu^2)}} \tag{4.9}$$

It must be emphasized that the initial condition taken here with a semi-infinite debonded zone favors interfacial crack propagation. In more realistic systems with defects or debonded zones of finite size at the interface between film and substrate (or bonding layer), such a level of compressive stress might not induce delamination. In addition, another mechanism must be taken into account to describe the delamination of films: buckling, frequently observed in thin film under compression, leads to modifications of the expression of the energy release rate G as given in Equation 4.8. In the following section, we focus on this process and the conditions for film buckling. The out of plane displacements of the film are then taken into consideration in order to predict propagation of the delamination crack. In all the following, we limit our analysis to a 2D geometry of the specimen [e.g. plane (O_{xy}) in Figure 4.1]. We consider defects of length $2a$ at the interface between film and substrate and determine if these debonded zones can grow and lead to catastrophic consequences for layer transfer.

4.5.2 Buckling of the Film

We consider the situation represented in Figure 4.3(a) where an initial defect or debonded zone of size $2a$ is present at the interface between the film and the substrate. Under a sufficiently high compressive stress, the film can buckle as shown in Figure 4.3(b), and a stability analysis of the film provides expression for the critical stress [44].

Consider now that the film is submitted to a given compressive stress σ_m. One can use this expression to show that buckling will occur if the delamination zone is larger than a critical size a_b, where:

$$a_b = \frac{\pi h}{2}\sqrt{\frac{E}{3(1-\nu^2)\,|\sigma_m|}} \tag{4.10}$$

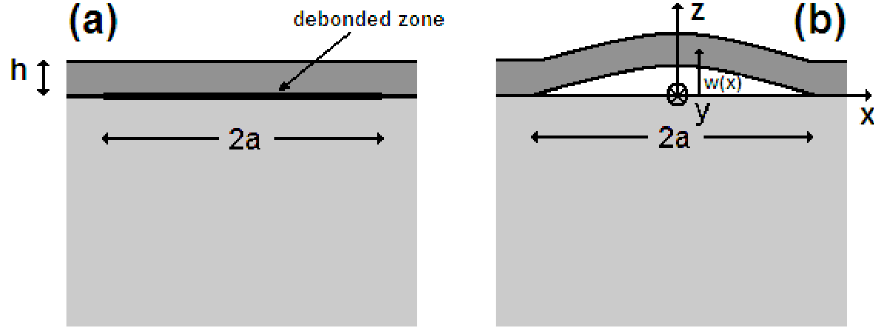

Figure 4.3. Two-dimensional profile of a debonded part of a film (a) without and (b) with buckling.

This process is energetically favorable because, in essence, it increases the effective length of the film.

4.5.3 Propagation of the Delamination Front Induced by Film Buckling

As mentioned previously, buckling of the film affects the energy release rate of the interfacial crack so that the buckling pattern must be taken into consideration when predicting the onset of delamination. In particular, the stress concentration at the edge of a debonded zone changes drastically with the size of the buckling zone. This effect is represented in Figure 4.4 where the variations in the energy release rate G are represented as a function of the half-length a of the debonded zone. For sufficiently large buckling zones, G might reach G_c and the interfacial crack can propagate. To assess the critical size a_p that allows a buckling pattern to propagate, one can derive the value of the energy release rate for a buckled zone of length $2a$ [44],

$$G(a) = \frac{\sigma_m^2(1-\nu^2)h}{2E}\left(1-\frac{a_b^2}{a^2}\right)\left(1+3\frac{a_b^2}{a^2}\right) \tag{4.11}$$

that is represented in Figure 4.3(b). It is interesting to note that at the onset of film buckling ($a = a_b$), there is no driving force for delamination ($G = 0$). However, if the compressive stress in the film is increased, the value of $a_b(\sigma_m)$ will decrease leading finally to a net increase in the delamination driving force. As a result, propagation is possible at a certain stress level when the condition $G(a) = G_c$ is satisfied. Solving the previous equation with respect to a, one obtains the critical length a_p above which the buckling zone will propagate,

$$a_p = \frac{\pi h}{2}\sqrt{\frac{E}{1-\nu^2}}\frac{1}{\sqrt{|\sigma_m|}}\frac{1}{\sqrt{1+\sqrt{4-\frac{6EG_c}{h(1-\nu^2)\sigma_m^2}}}} \tag{4.12}$$

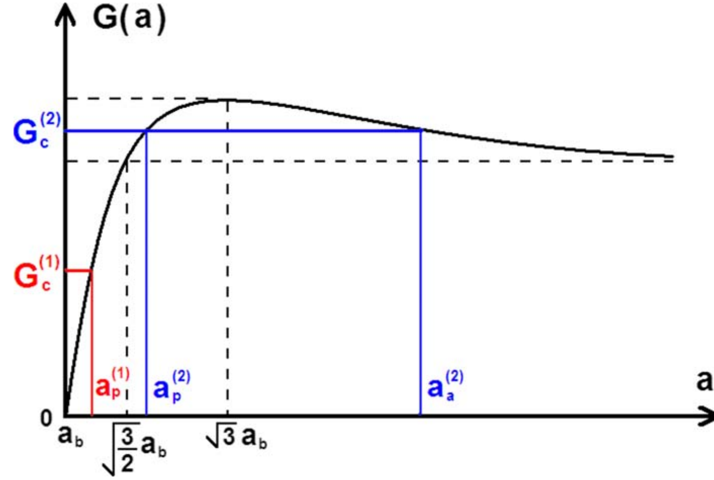

Figure 4.4. Variations in the energy release rate of an interfacial crack at the edge of a buckled zone of length $2a$ [Figure 4.3(b)]. $2a_b$ corresponds to the minimum length for a debonded zone in a film of the same thickness under the same compressive stress to buckle.

a_p being a decreasing function of $|\sigma_m|$, it is also clear in this representation that a sufficiently large compressive stress will induce delamination. Note that Equation 4.12 is only valid for $|\sigma_m| > \frac{\sqrt{3}}{2}\sigma_{del}$ where σ_{del} has been introduced in Equation 4.9. For smaller values of compressive stress $|\sigma_m|$ in the film, the buckling zone remains stable regardless of the initial size of the debonded zone.

However, the previous analysis is limited to crack initiation and to predict the full evolution of the system beyond initiation, it is important to separate two cases, as illustrated in Figure 4.4:

(1) If the critical length a_p for interfacial crack propagation is smaller than $\sqrt{\frac{3}{2}}a_b$, where a_b is the critical length for buckling [Equation 4.10], the equation $G_c = G(a)$ has only one solution a_p given by Equation 4.12, corresponding to the size of the smallest defect leading to crack initiation. The condition $G_c \geq G(a)$ for crack propagation begin satisfied whenever $a > a_p$, this situation corresponds to crack propagation without arrest.

(2) If the length a_p is larger than $\sqrt{\frac{3}{2}}a_b$, the equilibrium equation for debonding is satisfied for two crack lengths, a_p and a_a. The elastic energy released is larger than the fracture energy only for crack extensions between these two length scales so that initiation and crack arrest

occur successively for $a = a_p$ [Equation 4.12] and a_a, with:

$$a_a = \frac{\pi h}{2}\sqrt{\frac{E}{1-\nu^2}}\frac{1}{\sqrt{|\sigma_m|}}\frac{1}{\sqrt{1+\sqrt{4-3\left(\frac{\sigma_{del}}{\sigma_m}\right)^2}}} \tag{4.13}$$

The conditions for both situations can be rewritten in terms of stress, and and unstable crack propagation corresponds to $|\sigma_m| \geq \sigma_{del}$, while crack arrest will be observed if $\sigma_{del} > |\sigma_m| \geq \frac{\sqrt{3}}{2}\sigma_{del}$. The value of the defect length corresponding to $a_p = a_a$ is noted a_{del}, where:

$$a_{del} = \frac{\pi h^4}{2}\sqrt{\frac{2hE}{3G_c(1-\nu^2)}} \tag{4.14}$$

In both cases, the propagation of these interfacial cracks may adversely affect the quality of the transferred thin film. In particular, for sufficiently large buckled patterns, i.e., large enough interfacial crack extension, a transverse crack induced by the bending generated in the film can fracture the crystal layer. It is worth noting that this process may not occur for an interfacial failure with a small extension. The conditions to obtain such transverse cracks are now discussed in detail.

4.5.4 Failure of the Thin Film Induced by Bending

When buckling occurs, the delaminated zone undergoes bending. If the original debonded zone is sufficiently small, bending increases while the size of the buckling zone increases. For a sufficiently large buckling zone, the film is not strong enough to support the tensile stress induced by bending in the film and a crack initiating from the upper surface of the film in $x = 0$ will propagate parallel to the y axis toward lower surface [Figure 4.3(b)]. In this geometry, crack propagation is expected to be without arrest, and propagation will occur throughout the crystal layer.

To predict the onset of crack initiation, we use a criterion based on the value of the curvature of the film (akin to critical strain), as e.g. in Ref. 15: failure occurs when the curvature $\frac{d^2w}{dx^2}$ at some point of the film exceeds the critical value $\frac{1}{R_c}$, where R_c is a constant depending not only on the intrinsic strength of the material but also on the state of surface of the freshly cut crystal. As seen in Figure 4.3(b), a possible transverse crack will initiate around $x = 0$ where the local curvature of the film is maximum. The deflection $w(x)$ of the film is then expressed in terms of the delaminated zone size $2a$ and the compressive stress σ_m (e.g., Ref. 4), providing an expression for

the maximum curvature $\left.\frac{d^2w}{dx^2}\right|_{x=0}$ of the film. From this expression and the curvature based failure criterion introduced previously, one can show that transverse failure occurs for buckled thin film larger than a_f, with:

$$a_f = \pi \sqrt[4]{3(1-\nu^2)}\sqrt{hR_c}\sqrt{\frac{|\sigma_m|}{\sigma_l}}\sqrt{1-\sqrt{1-\left(\frac{\sigma_l}{\sigma_m}\right)^2}} \tag{4.15}$$

where

$$\sigma_l = \frac{E}{2\sqrt{3(1-\nu^2)}}\frac{h}{R_c} \tag{4.16}$$

Note that the film failure is impossible if $|\sigma_m| < \sigma_l$, regardless of the size of the debonded zone. For $|\sigma_m| = \sigma_l$, we introduce the size $a_l = a_f(\sigma_l)$ of the smallest debonded zone for which failure will occur

$$a_l = \pi \sqrt[4]{3(1-\nu^2)}\sqrt{hR_c} \tag{4.17}$$

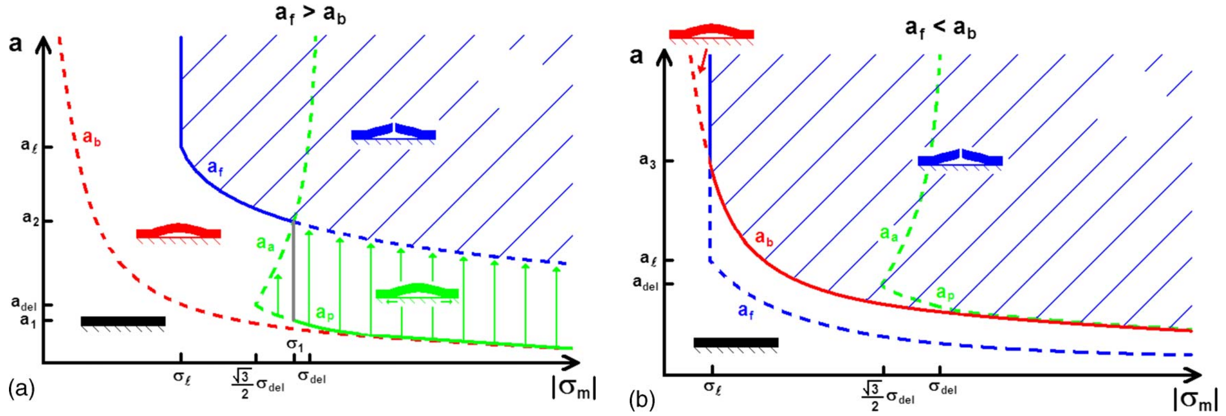

Figure 4.5. Diagrams representing the state of the system and its evolution during the layer transfer process in two different cases; (a) film with high resistance to failure/small thickness ($a_f > a_b$); (b) film with low resistance/large thickness ($a_f < a_b$). Buckling, delamination, and film failure correspond to the domains above the dotted red line $a_b(|\sigma_m|)$, to the vertical green arrows, and the hatched blue domain, respectively. Film cracking is avoided if the system remains in a state located below the solid line in this representation.

4.5.5 Comparisons of the Various Length Scales of the Problem and Criterion for Film Failure

In the preceding paragraphs, the criteria for film buckling, extension of the debonded zone, and transverse failure of the film were expressed in terms of debonded zone size. In these three cases, it was possible to define a critical size above which the process is expected to occur. For the specific case of propagation of the delamination front, our analysis showed that above a critical length, the process will stop. These critical debonded sizes were shown to depend on the applied stress in the film, and their dependence on σ_m was explicitly given in Equations 4.10, 4.12, and 4.15.

To be able to predict in a simple way film failure during layer transfer, these three criteria are represented on a same graph in Figure 4.5 where the compressive stress $|\sigma_m|$ in the film is given along the abscissa and the half-length a of the debonded zone is given along the ordinate. In this representation, the state of the system at a given time corresponds to the point $(|\sigma_m|,a)$. For each process studied, i.e., buckling, delamination, and film failure, the space $(|\sigma_m|,a)$ can be divided into two distinct regions, separated by the curves $a_b(|\sigma_m|)$, $\{a_p(|\sigma_m|),\ a_a(|\sigma_m|)\}$, and $a_f(|\sigma_m|)$. If the system, characterized by its coordinates $(|\sigma_m|,\ a)$ is in the region defined for a given process, then this process will occur, while if the system corresponds to a point lower than the critical curve defined for the phenomenon, one does not expect this process to occur. Therefore, this relatively simple representation can be used to follow the temporal evolution of the layered specimen.

Such diagrams are represented in Figure 4.5 where the critical defect length $a_b(|\sigma_m|)$ for buckling, $a_p(|\sigma_m|)$ and $a_a(|\sigma_m|)$ for propagation and arrest of the delamination front, and $a_f(|\sigma_m|)$ for film failure are plotted. The relative position of the curves defining the domain for buckling and delamination is robust and independent of the specific value of the parameters of the problem. In particular, the critical length for buckling a_b is always smaller than the critical length for interfacial crack propagation a_p, and in the limit of large compressive stress, $a_b \simeq a_p$. However, the position of the domain corresponding to film failure with respect to these curves may change with the value of the parameters. For illustrative purposes, two cases have been considered: on Figure 4.5(a), the critical length for failure a_f is larger than those at buckling a_b and delamination a_p. This corresponds to thick films and/or a highly resistant films. The other system, corresponding to Figure 4.5(b), is for thin films and/or films with little resistance to cracking and/or films with a large critical radius of curvature R_c at failure.

In both diagrams, the hatched zone corresponds to states of the system where the film is

broken. Propagation of the interfacial crack, and thus the extent of the debonded zone, is indicated by vertical arrows.

We first consider the case of a highly resistant film with a small thickness Figure 4.5(a). Whatever the initial size a_{ini} of the largest defects at the bonding interface, one can follow the evolution of the system during the layer transfer process. For example, let us take an initial defect with size a_{del}. During layer transfer, the temperature is increased and as a result, the stress $|\sigma_m|$ in the film also increases according to Equation 4.1. At the start of the process, the system evolution is represented by a horizontal line because the debonded zone remains unchanged. When the system reached the line $a_b(|\sigma_m|)$ demarcating the flat film and the film buckling, this zone starts to buckle but a still remains constant, so the specimen evolution can still be represented by a horizontal line. When the system reaches the line $a_p(|\sigma_m|)$, demarcating the stable buckled film and the propagation of the interfacial crack, there is delamination of the film and a increases. Therefore, a vertical line now describes the evolution of the film geometry. Two cases are then possible: (i) if the initial defect was sufficiently small ($a < a_1$), the extension of the buckled domain leads to film failure. In this case, the trajectory of the system in this representation reaches the border of the hatched zone. Here, the critical debonded zone size before the appearance of transverse cracks is provided by $a_p(|\sigma_m| \geq \sigma_1)$ (represented as a solid line); (ii) the crack stops before film failure, leading to a debonded zone of size a_a which is smaller than the critical length for failure a_f. The system will fail only if the temperature is increased again, resulting in a quasistatic propagation of the delamination crack with half-length a_a. Transverse cracks will eventually initiate if the compressive stress is sufficiently high so that $a_a(|\sigma_m|)$ reaches the critical size for failure a_f. In this case, the critical compressive stress σ_1 for film cracking is given by $a_a(\sigma_1) = a_f(\sigma_1) = a_2$. Defining $a_1 = a_p(\sigma_1)$, one arrives at the following variations in the maximum admissible compressive stress σ_c with the initial defect size:

(i) For $a_{ini} < a_1$, one gets $\sigma_c = a_p^{-1}(a_{ini})$, where $a_p(\sigma)$ is provided by Equation 4.12;

(ii) For $a_1 < a_{ini} < a_2$, one gets $\sigma_c = \sigma_1$;

(iii) For $a_2 < a_{ini} < a_l$, one gets $\sigma_c = a_f^{-1}(a_{ini})$, where $a_f(\sigma)$ is provided by Equation 4.15;

(iv) For $a_l < a_{ini}$, one gets $\sigma_c = \sigma_l$ given in Equation 4.16.

Let us now focus on the case of films with large thicknesses and/or low resistance to failure. From the analysis of the corresponding diagram presented in Figure 4.5(b), two cases can be isolated:

(i) for initial defects smaller than $a_3 = a_b(\sigma_l)$, the film remains intact as long as the critical stress for buckling is not reached. At this threshold, the debonded zone starts to buckle and a transverse crack appears at the same time. This means that the critical stress σ_c for film failure is provided by the expression for the buckling stress of a debonded zone of size a_{ini} that can be derived from Equation 4.10; (ii) for larger initial defects $a_{ini} > a_3$, the film first buckles and then breaks when the compressive stress reaches the critical stress for failure σ_c. This leads us to conclude that:

(i) for $a_{ini} < a_3$, one gets $\sigma_c = \frac{\pi^2}{12}\frac{E}{1-\nu^2}\left(\frac{h}{a_{ini}}\right)^2$;

(ii) for $a_3 < a_{ini}$, one gets $\sigma_c = \sigma_l$ given in Equation 4.16.

It is interesting to note that in the limit of very small defects $a \ll a_{del}$, both kinds of systems, represented by two rather different diagrams lead to the same expression for the critical compressive stress for film cracking. Using the approximation $a_b \simeq a_p$ valid for large compressive stress, one gets in both cases $\sigma_c \simeq \frac{\pi^2}{12}\frac{E}{1-\nu^2}\left(\frac{h}{a_{ini}}\right)^2$. The same remark is also valid in the limit of large defects for which $\sigma_c = \sigma_l = \frac{E}{2\sqrt{3(1-\nu^2)}}\frac{h}{R_c}$.

This analysis provides an upper limit σ_c to the compressive stress that can be imposed on the film. Conversely using Equation 4.1, the maximum layer transfer temperature to which the system can be exposed to avoid failure can be also predicted. With the result obtained in Section 4.4 from the stability analysis of microcracks leading to film splitting, one gets a range of admissible stress $-\sigma_c < \sigma_m < 0$ for the system during the layer transfer process, each limit corresponding to distinct failure modes. The theoretical predictions are compared with experimental observations in Section 4.6.

4.6 Discussion and Comparison with Experimental Results

To determine to what extent the previous analysis applies to experimental situations, two kinds of experiments for which transverse cracks in the film were observed have been analyzed. Each one corresponds to one failure mechanism analyzed in the previous sections. The first experiment is devoted to the study of the stability of microcracks in the film and analyzes the effect of the tensile/compressive state of stress on their trajectory. The second experiment has been designed to study the effect of large compressive stresses on the film.

4.6.1 Effect of the Compressive/Tensile State of the Stress on the Stability of Cracks

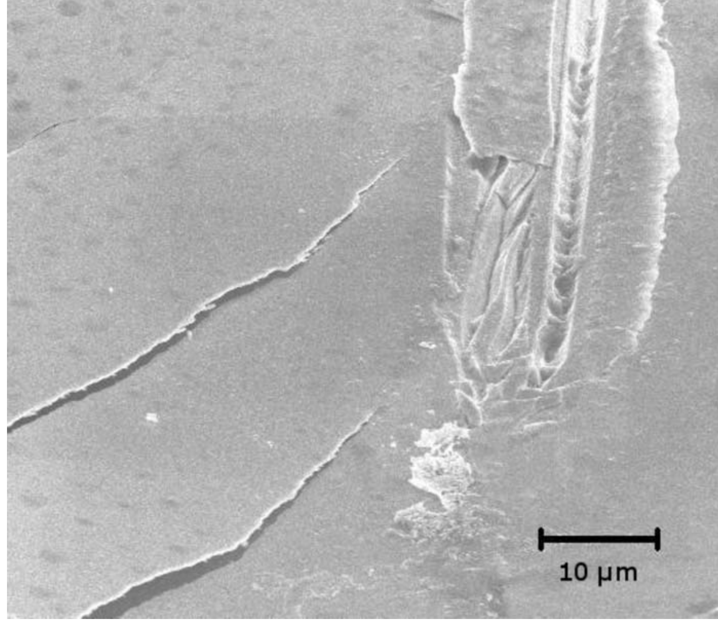

Figure 4.6. SEM image of the top surface of an ion implanted $LiNbO_3$ sample after heating without being bonded to a substrate. Transverse cracks can be seen coming from the implanted region in the $LiNbO_3$, through the thin film, and emerging on the top surface of the sample.

For the first experiment, a sample of lithium niobate ($LiNbO_3$) was implanted with hydrogen and helium to a depth of h = 400 nm below the top surface. The specimen was heated and no bonding was involved. In this case, a coherent thin film of $LiNbO_3$ is not separated from the rest of the material; rather, the cracks that initiated at the plane of implantation immediately deviate from a horizontal trajectory and finally emerge at the top surface of the sample Figure 4.6.

To explain these results, we assess the effect of the absence of substrate on the stress state in the $LiNbO_3$ specimen: the stress σ_m remains equal to zero even during the heating phase. Therefore, the cracks initiating from the implanted plane are unstable and as discussed in Section 4.4, they are expected to deviate from a horizontal trajectory. This observation is in agreement with the condition $\sigma_m < 0$ that was proposed in Section 4.4 to ensure successful layer transfer.

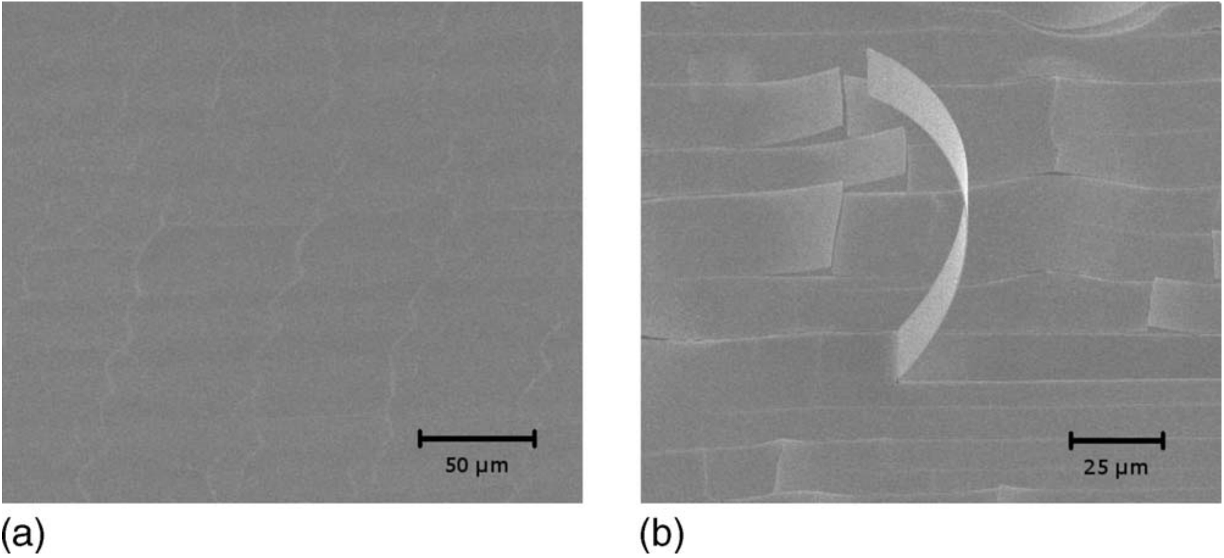

Figure 4.7. SEM image of the free surface of the transferred thin film. (a) One can see a network of parallel fractures with telephone-cord-like cracks which are characteristic of buckling instabilities; (b) one can observe the network of secondary cracks perpendicular to the wavy cracks, also produced by buckling and failure of the film.

4.6.2 Effect of a High Compressive Stress on the Film

The second experiment was performed on a system whose geometry corresponds to that represented in Figure 4.1. The crystal to be transferred is again ion implanted $LiNbO_3$ with h = 400 nm. The $LiNbO_3$ and silicon (Si) substrate were bonded together with minimal pressure and a silver bonding layer which will be discussed in Chapter 5 [32]. The substrate, the bonding layer, and the $LiNbO_3$ specimen have square bases with sides of 1 cm. The thickness of the substrate and the bonding layer are 1 mm and 800 nm, respectively. The system is then heated up to 750 K so that $\Delta K \simeq 450$ K, leading to a compressive stress in the film from the mismatch in thermal expansion coefficients, $\alpha_{\mathrm{LiNbO_3}}$ being larger than α_{Si}. In this case, layer transfer of the $LiNbO_3$ specimen is obtained. This demonstrates that the compressive stress induced by the bonding of $LiNbO_3$ onto a substrate with a smaller thermal expansion coefficient has enabled crack propagation along the plane of implantation. This agrees with the predictions of Section 4.4. SEM images of the transferred $LiNbO_3$ thin film indicate the presence of transverse cracks that have cut the film in various pieces Figure 4.7. One can see that these transverse cracks are all oriented in the same direction. This might correspond to the direction normal to the one of maximum thermal expansion within the

$LiNbO_3$[6]. Also, these cracks follow a wavy trajectory, also referred to as "telephone-cord-like" patterns, characteristic of thin film buckling [28, 91]. This is strong evidence in support of the predictions of Section 4.5: at first, the thin film buckles from a highly compressive stress, resulting in a network of buckling zones with a characteristic wavy geometry. Then, failure occurs by bending of the film where debonding has occurred. This leads to transverse cracking in the film with the same wavy structure as the buckling.

An additional observation suggests that the transverse cracks observed in the film do not come from the deviation of microcracks which initiate at the plane of ion implantation, but result from buckling, delamination, and then failure of the film. The study of the other part of the sample ($LiNbO_3$) that has been separated from the rest of the layered structure does not reveal any cracks on the freshly created surface. In other words, the interface between film and substrate plays a crucial role in the initiation of these undesirable cracks, while ion implantation leads to a controlled splitting of the film when bonded to a substrate with a smaller thermal expansion coefficient. This observation also suggests that a controlled splitting of the $LiNbO_3$ single crystal is not enough to obtain a defect-free thin film, and the formation of transverse cracks by processes after layer transfer is also possible, as shown in Section 4.5.

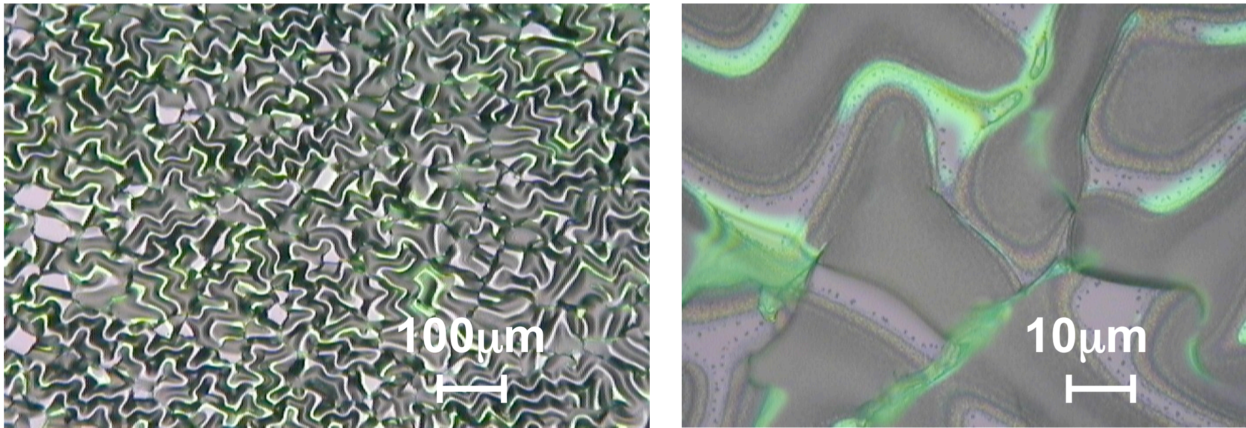

Figure 4.8. The left and right panels represent optical microscopy images of layer transfered $LiNbO_3$ under excessive compressive stress.

Another striking example of a film under excessive compressive stress is shown in Figure 4.8.

[6]The thermal expansion coefficients of the $LiNbO_3$ crystal are different along the various crystalline directions.

During the layer transfer process, this sample was in a state of compressive stress that enabled buckling of the film; however, the state of stress was not high enough to drive the buckled regions to the point of failure. This corresponds to the region of 4.5(a) between the red and a_b and a_f curves.

We now quantitatively compare the observations made in this experiment with the theoretical predictions made in Section 4.5. In order to estimate the compressive stress at failure in the $LiNbO_3$ film, Youngs modulus, and Poissons ratio of $LiNbO_3$ are taken to be E = 150 GPa and $\nu = 0.32$, close to the values measured for similar materials [51, 64]. The thermal expansion coefficients of Si and $LiNbO_3$ are $\alpha_{Si} = 2.6x10^{-6}$ K^{-1} and $\alpha_{\mathrm{LiNbO_3}} = 8.2x10^{-6}$ K^{-1} [58], respectively, leading to $\Delta\alpha = -5.6x10^{-6}$ K^{-1}. The critical radius of curvature for film failure under bending is estimated to be $R_c \simeq 1$ cm. Even though this value is a rather rough estimate, it is important to note that the shape of the curve a_f is rather insensitive to the value of R_c in the range of interest $|\sigma_m| > 0.1$ GPa[7]. Ceramic materials that are bonded to silver layers exhibit fracture energies on the order of $G_c \simeq 1 - 2$ J m^{-2}. In the following, we have kept the fracture energy as a free parameter and chosen the value that enables the best agreement between experimental observations and theoretical predictions. The value so obtained is then compared with the expected values for ceramic-silver fracture energy.

Using the previous numerical values and Equation 4.1, it is possible to estimate the compressive stress $\sigma_{failure} \simeq 0.57$ GPa in the film at $T \simeq 750$ K for which undesired cracks appear. For the $LiNbO_3$/Ag/Si system studied here, one can also calculate the failure diagram to determine the state of the system with respect to $|\sigma_m|$ and a Figure 4.9. To reproduce correctly the experimental observations, one chooses $G_c \simeq 0.5$ J m^{-2} that is smaller but comparable to the expected values $G_c \simeq 1 - 2$ J m^{-2}. The resulting diagram is analogous to Figure 4.5(a), which is plotted for the general case. The value of the compressive stress at $T \simeq 750$ K is also represented on this diagram as a vertical dashed line. It is now possible to identify the different processes that have led to the failure of the film. Using the representation of the system state shown in Figure 4.9, the initiation of the transverse cracks in the film is given by the intersection of the vertical dashed line giving the level of stress at film failure with the curve $a_f(|\sigma_m|)$. This line represents the boundary between intact and broken films. This provides a reasonable estimate $a \simeq 8$ μm of the size for the defects at the interface between the silver bonding layer and the $LiNbO_3$ film that will ultimately lead to

[7]From the expression of a_f given in Equation 4.15, one can see that this length becomes independent of σ_m for large values of the stress in the film.

undesirable cracks in the film.

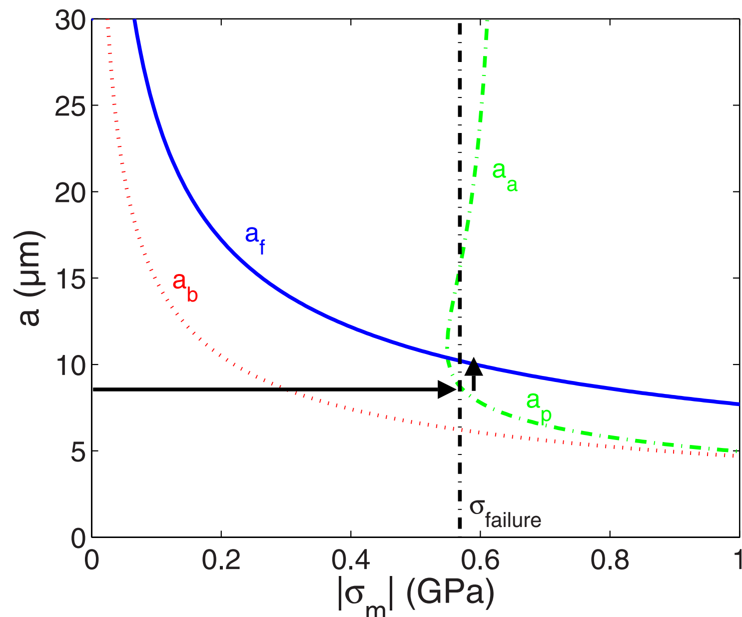

Figure 4.9. Diagram representing the evolution of the $LiNbO_3$/Ag/Si system during the later transfer process. The vertical line is the experimental compressive stress $\sigma_{failure} \simeq 0.57$ GPa in the film at failure, while the red dotted, green dashed, and blue solid curves correspond to the theoretically predicted critical values of the delaminated zone size for film bending, interfacial crack propagation/arrest, and film failure, respectively. The predicted evolution of the experimental system during layer transfer is represented by the black arrows.

From this diagram, one can also follow the temporal evolution of the film failure during the heating phase. The evolution of the system during the initial phase is described by the horizontal arrow represented in Figure 4.9. The defects at the interface between Ag and $LiNbO_3$ of size $a \simeq 8$ μm will start to buckle for $\sigma_m \simeq 0.3$ GPa (corresponding to a temperature of $\simeq 540$ K). This value is given by the intersection of the horizontal arrow with the curve a_b. When the compressive stress in the film is sufficiently high, close to $\sigma_{failure}$, the interfacial cracks start to propagate. A network of debonded zones with a telephone-cord-like geometry then develops. This process will ultimately lead to the telephonecord-like cracks observed postmortem on the thin film surface [Figure 4.7(a) when the debonded zones start to extend in the transverse direction[8]. The evolution of the system

[8]This expansion of the debonded zone in two stages might be explained by a slight anisotropy of the thermal expansion coefficienty of the $LiNbO_3$ single crystal. In the first stage, the compressive stress, larger along one of the crystallographic orientations of the $LiNbO_3$, produces and extension of the initial defects - converted into circular

in this last regime is described by the vertical arrow represented in Figure 4.9. Finally, failure of the film, which corresponds to the intersection of the vertical arrow with the curve a_f, is obtained for for debonded zones with lateral dimensions on the order of $a \simeq 10\ \mu m$. This is fully compatible with the postmortem observations made on the film surface after layer transfer.

4.7 Conclusion

In this chapter the origin of the undesirable cracking during layer transfer has been investigated. From our theoretical analysis based on fracture mechanics, it appears that the state of stress in the film, a direct consequence of the mismatch between the thermal expansion coefficients of the film and the substrate, drives the failure process. In addition, two phenomena identified in experimental tests are studied in detail and shown to induce catastrophic failure of thin films obtained by layer transfer: (i) the microcracks that propagate in the implanted plane parallel to the film/substrate interface and split the specimen can deviate from their horizontal trajectory and cut the film. The analysis of their stability in 3D shows that these microcracks will follow a straight crack path if the film is submitted to a compressive stress $\sigma_m < 0$; (ii) if the compressive stresses within the layer transfered thin film are above a critical value, the bonding and layer transfer process will fail. When the specimen is already cut but still heated, defects at the film-substrate interface can induce film buckling and delamination, ultimately resulting in film failure from bending. This process has been analyzed in detail, and the critical stresses (critical temperatures) at which each stage occurs have been expressed in term of defect size, film thickness and fracture properties of the film. Therefore, it is possible to predict the maximum compressive stress σ_c that can be sustained by the system. Taking into consideration both of these failure processes, one can define a range of acceptable stresses $-\sigma_c < \sigma_m < 0$ within the film.

From these results, it is now possible to identify the systems for which the layer transfer process will be successful. In particular, the the acceptable film stresses can be calculated in terms of the materials, bonding layers, and sample thicknesses being used. The substrate must be chosen so that its thermal expansion coefficient is smaller than that of the film. But this condition is not sufficient and above a critical temperature, which corresponds to a compressive stress σ_c, the transfered film will be cracked. This temperature must be lower than that necessary to make the

debonded zones - into telephone-cord-like patterns that toes not accompany an increase in the maximum curvature of the buckled zones. This is the case in the second stage characterized by a lateral expansion of these zones that produce film failure

microcracks propagate in the implanted plane of the film. To overcome this difficulty and increase the admissible stress in the film, the quality of the interface between film and substrate must be improved, decreasing both the defect size and increasing the interfacial fracture energy. One way to achieve a successfully transfered layer is by increasing the film thickness. A second alternative is to use a deformable plastic interlayer (e.g., Au, Ag, and Cu) which can increase bond strength and the chance of a successful bond. This is the focus of Chapter 5.